
Article:
Li, G. orcid.org/0000-0002-5956-4033, Ren, B., Zhu, Z.Q. et al. (2 more authors) (2017) Demagnetization withstand capability enhancement of surface mounted PM machines using stator modularity. IEEE Transactions on Industry Applications. ISSN 0093-9994

10.1109/TIA.2017.2777922

Demagnetization Withstand Capability Enhancement of Surface Mounted PM Machines Using Stator Modularity

G. J. Li, Senior Member, IEEE, B. Ren, Z. Q. Zhu, Fellow, IEEE, M. P. Foster, and D. A. Stone

Abstract —The flux gaps in alternate stator teeth of the modular PM machines can have a significant impact on the total magnet flux density, and hence, the potential magnet reversible/irreversible demagnetization under flux weakening operations or short-circuit conditions. Such a problem has not been studied in literature and will be investigated in this paper. The influence of flux gaps on the d-axis inductance and the potential peak short-circuit current is analysed for different slot/pole number combinations. It is found that the flux gaps will affect both the d-axis inductance and open-circuit flux linkage, and hence reduce short-circuit current of machines with pole number (2p) smaller than slot number (N_s) while they will increase the short-circuit current of machines with $2p > N_s$. However, the opposite phenomena can be observed for demagnetization withstand capability. For machines having $2p < N_s$, the flux gaps tend to lower withstand capability, whilst for machines having $2p > N_s$, this capability can be improved. Other parameters, such as magnet thickness, temperature, etc., have also been accounted for in the demagnetization analysis. Tests have been carried out to validate the predictions of inductances and short-circuit current as well as performance such as phase back-EMF, cogging torque and static torque for machines with one defective magnet, which represents the case of partially demagnetized magnets.

Index Terms — demagnetization withstand capability, flux gap, modular machine, permanent magnet, short-circuit current.

I. INTRODUCTION

DUE to higher torque density and efficiency compared to other machines such as switched reluctance machines and induction machines, permanent magnet (PM) machines are being widely used in a variety of applications ranging from domestic appliances, automotive to renewable energy such as tidal and wind power, etc. In order to improve the fault tolerance capability and also to simplify the manufacturing process, particularly for large PM machines, the modular topologies (segmented stator and/or rotor) have been introduced in the last decades [1] [2] [3] [4]. Due to the specific segmented stators, these modular machines can overcome the main drawbacks of conventional modular machines such as reduced average torque and increased torque ripple [5] [6]. This is mainly due to the fact that the flux gaps in alternate stator teeth as shown in Fig. 1 can introduce a threefold effect on winding factor, open-circuit air-gap flux density and flux focusing or defocusing. As a result, with properly selected slot/pole number combinations and flux gap widths, the average torque can be increased and the torque ripple can be mitigated [4].

However, as other PM machines, the modular ones also face the demagnetization problems. The mechanisms of the PM demagnetization are detailed in [7]. Several factors that cause the PM demagnetization can be summarized: 1) demagnetizing flux due to flux weakening operations or short-circuit conditions [8] [9]; 2) over heating [10], [11], [12]; 3) PM material oxidation, corrosion or damaging [11], etc.

Compared to the flux weakening, the short-circuit faults are even more problematic because the short-circuit current could be several times larger than the rated current, particularly during transient state, and hence cause serious over heating problems. This tends to reduce the remanence and the coecivity of magnets whilst additionally increasing their knee points (easier to be irreversibly demagnetized), particularly for rare earth magnets such as NdFeB. Consequently, the magnet demagnetization withstand capability will deteriorate. In addition, the short-circuit current, at high speed in particular, can be regarded as a d-axis current and hence a demagnetizing current, which will move the magnet working point closer to the knee point, and therefore aggravate even further the demagnetization withstand capability.

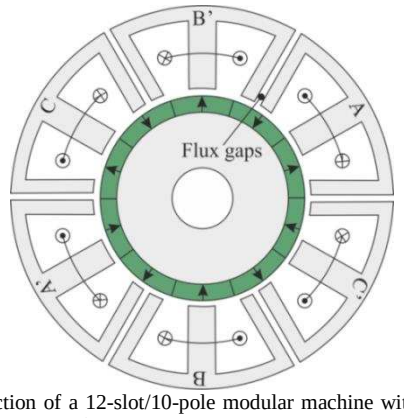

Fig. 1 Cross-section of a 12-slot/10-pole modular machine with 6 single layer concentrated windings. 6 flux gaps are in stator teeth without windings [13].

TABLE I PARAMETERS OF THE INVESTIGATED MACHINES

Slot number	12	Number of turns/phase	132
Pole number	10/14	Rated current (A_{rms})	7.34
Stator outer radius (mm)	50	Rated speed (rpm)	400
Stack length (mm)	50	Magnet remanence (T, 20°C)	1.2
Air-gap length (mm)	1	Knee point (T, 20°C)	-0.08
Magnet thickness (mm)	3		

It is worth mentioning that most of the existing studies on demagnetization issues are for conventional non-modular PM machines. So far no such study has been reported for modular PM machines. Therefore, this paper is dedicated to fill in this gap. Since the flux gaps dramatically modify the main magnetic circuit of modular machines, the armature magneto-motive force (MMF) and the air-gap flux density due to permanent magnets are changed accordingly. Moreover, the specific modular topologies require employing fractional slot concentrated windings. This also introduces a large number of sub- and

super-harmonics in stator MMF, leading to increasing risk of magnet partial irreversible demagnetization [14].

Therefore, more specifically, this paper will investigate the influence of flux gaps on the achievable short-circuit current and the irreversible demagnetization of modular machines due to this short-circuit current. The parameters that influence the magnet demagnetization such as slot/pole number combination, machine operating temperatures and magnet thickness and so on will also be taken into account. The frozen permeability (FP) method will be employed in order to separate the magnet flux densities due to armature MMF and magnets themselves, and hence the influence of flux gaps on both flux densities can be accurately analysed [15]. Finally, regarding the experimental validations, in order to simulate the partial demagnetization in a controllable manner, a modular PM machine with defective rotor (half of a magnet pole is removed) has been used in this paper.

II. Short-Circuit Current Analysis

The d-axis current under flux weakening operations and the short-circuit current, the latter in particular, are the main cause of magnet irreversible demagnetization. Therefore, it is essential to predict the maximum allowable short-circuit current of a designed PM machines in order to avoid the potential magnet irreversible demagnetization. In this paper, unless it is specifically pointed out, the machine operating temperature is 20°C. However, the influence of different temperatures on demagnetization will be investigated in the section III.

A. Influence of Flux Gaps on D-Axis Inductance

When a 3-phase short-circuit occurs, if the rotor speed is high enough so that the influence of phase resistance can be neglected, the highest steady-state short-circuit current (I_{SC}) for permanent magnet machines can be regarded as a d-axis current (I_d), and described by

$$I_{sc} = \sqrt{I_d^2 + I_q^2} \approx |I_d| = \frac{\Phi_0}{L_d} \tag{1}$$

where I_q is q-axis current, L_d is d-axis inductance and Φ_0 is the flux linkage due to permanent magnets, respectively.

It can be seen from (1) that to predict the I_{SC}, both L_d and Φ_0 need to be calculated first. Due to the magnetic saturation and armature reaction, the working point of PMs will be changed at different machine operating points (different speeds and torques). Therefore, Φ_0 and L_d are both load dependent variables and need to be accurately calculated using the FP method [15]. Using nonlinear two-dimensional finite element method (2D FEM) and the FP method, as well as the parameters given in TABLE I, L_d has been calculated for different I_d and flux gap widths, and compared in Fig. 2 (a). It is worth mentioning that the 12-slot/14-pole modular machine has similar d-axis inductance variation as the 12-slot/10-pole modular machine and is therefore not shown here. In addition, only negative I_d is considered, because they are similar to short-circuit current and will contribute to the magnet demagnetization. It can be found that L_d first reduces with the flux gap width then increases thereafter. However, the influence of I_d on L_d is marginal and hence can be neglected. This is mainly due to a relatively large effective air-gap length which limited the influence of armature reaction on magnetic saturation.

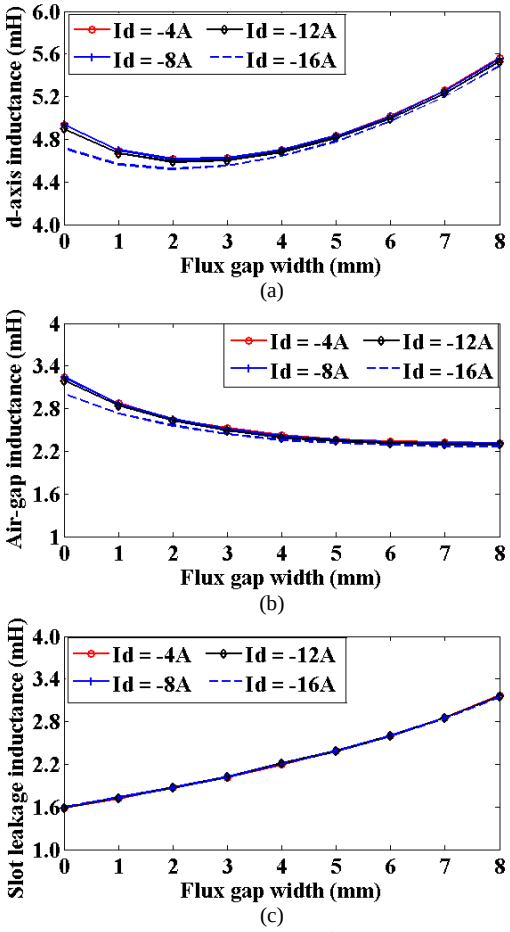

Fig. 2 d-axis inductance components vs flux gap width and I_d of the 12-slot/10-pole modular machine. (a) L_d, (b) fundamental air-gap inductance, (c) slot leakage inductance.

The following section is devoted to explain why L_d varies as shown in Fig. 2 (a). Without considering fringing and end-winding leakage inductances, the simplified expression of L_d accounting for both the air-gap fundamental inductance and slot leakage inductance [1st and 2nd terms on the right hand side of (2), respectively] can be described by [16]:

$$L_d \approx \frac{q\mu_0 (NK_{w1})^2 Dl}{\pi p^2 (g + l_m)} + N_s N_c^2 l \left(\mu_0 \frac{1}{3} \frac{d}{w}\right) \tag{2}$$

where q is the number of phases, μ_0 is the vacuum permeability, N is the number of series connected turns per phase, K_{w1} is the fundamental winding factor, D is the air-gap diameter, l is the stack length, p is the pole pair number, g is the mechanical clearance, l_m is the magnet thickness, N_s is the slot number, N_c is the number of conductors per slot, d is the slot depth and w is the average width of stator slot. For simplicity, the stator slots are assumed to be trapezoidal.

At d-axis position and with the 3 phases supplied by d-axis current, the air-gap fundamental flux can be roughly calculated by integrating the air-gap flux density due to armature field only over one slot pitch of the phase A. Subsequently, the fundamental air-gap inductance can be derived as shown in Fig. 2 (b). Subtracting the obtained fundamental air-gap inductance

from the total d-axis inductance, the slot leakage inductance can be obtained, as shown in Fig. 2 (c). It is found that the fundamental air-gap inductance reduces significantly while the slot leakage inductance increases almost linearly with the increasing flux gap width. The reduction of air-gap inductances is mainly due to the fact that the increasing flux gap width leads to the increase in effective air-gap length (g) as described by (2). However, the increase in slot leakage inductance is mainly due to the reduction of average slot width (w).

B. Influence of Flux Gaps on Short-Circuit Current

The PM (d-axis) flux linkages of the 12-slot/10-pole and the 12-slot/14-pole modular machines have been calculated by using the aforementioned FP method as well, and compared in Fig. 3 (a). Due to the influence of flux gaps on winding factor and air-gap flux density as demonstrated in [4], the PM flux linkage of the 12-slot/10-pole machine reduces steadily with the increasing flux gap width. However, the PM flux linkage of the 12-slot/14-pole machine increases to its maximum then reduces slightly thereafter. These different influences of flux gaps on d-axis inductances and PM flux linkages result in different short-circuit currents, as shown in Fig. 3 (b), which is akin to the PM flux linkage variation, as shown in Fig. 3 (a).

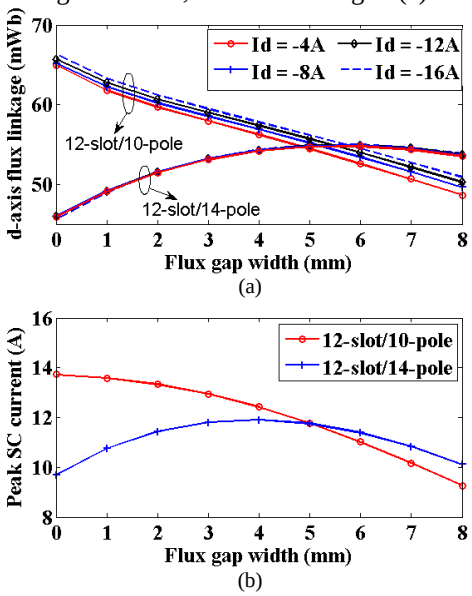

Fig. 3 PM (d-axis) flux linkages and the corresponding short-circuit currents vs flux gap width. (a) PM flux linkages, (b) short-circuit currents.

It is worth noting that the calculated short-circuit current is under steady-state. However, during transient state the peak short-circuit current could be much higher. A simple Matlab/Simulink model has been built to simulate the 3-phase short-circuit condition under generator mode. A rotor speed of 4000 rpm has been used, which is high enough to allow the modular machine to reach its peak short-circuit current. The predicted short-circuit currents are shown in Fig. 4. It can be seen that after the short-circuit, d-axis current reduces quickly after reaching its peak value, this is due to the fast attenuation of the transient current component. To simplify the investigation for both the short-circuit and flux weakening operations, a maximum I_{SC} up to -16A is chosen for the demagnetization analysis in this paper. However, it is worth mentioning that a higher short circuit current might result in even heavier magnet irreversible demagnetization.

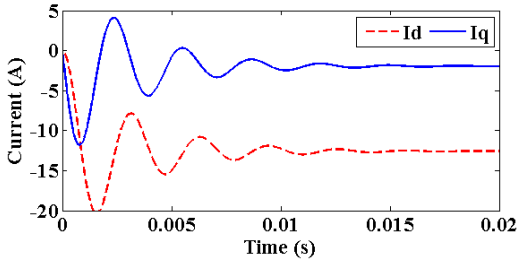

Fig. 4 Transient short-circuit currents (I_d and I_q) after 3-phase short-circuit under generator mode.

III. Demagnetization Analysis of Modular Machines

A. Influence of Demagnetizing Current

Under on-load conditions, the flux density within magnets can be calculated using a simplified analytical expression as described by (3). If B_m is below the knee point of magnet B(H) curve, one can conclude that the magnet is irreversibly demagnetized.

$$B_m = -\frac{\mu_0 \mu_r N I \beta}{l_m(\beta + \mu_r)} + \frac{B_r \beta}{(\beta + \mu_r)} \tag{3}$$

where $\beta = \frac{A_g l_m}{A_m l_g}$ is a permeance coefficient, A_g and A_m are the airgap and magnet areas, l_g and l_m are the airgap length and the PM thickness, N is the number of turns and I is the current, μ_r is the recoil permeability and B_r is the remenance of magnets.

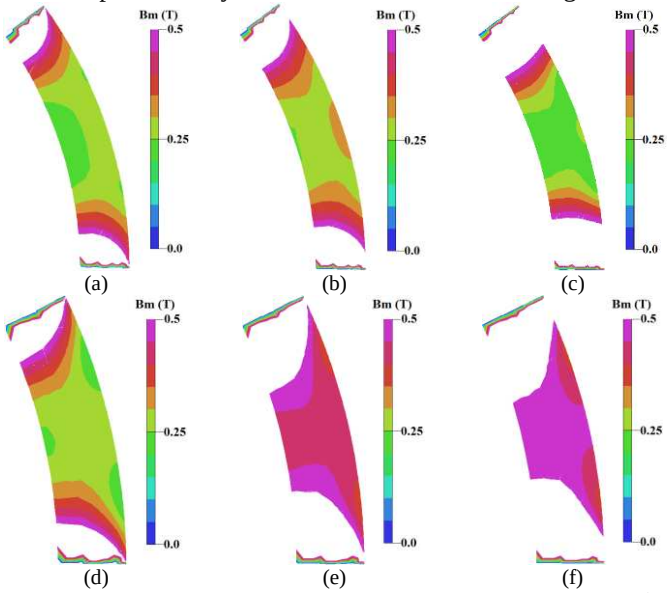

Fig. 5 B_m distribution within one PM. The empty area in the magnet has flux density above 0.5 T, therefore not demagnetized. The current is I_d = -16A and the rotor is at d-axis position. (a) FG = 0 mm (12/10), (b) FG = 4 mm (12/10), (c) FG = 8 mm (12/10), (d) FG = 0 mm (12/14), (e) FG = 4 mm (12/14), (f) FG = 8 mm (12/14). FG stands for flux gap width.

The B_m in one magnet for different flux gap widths and slot/pole number combinations have been calculated and compared in Fig. 5. The magnet thickness is 3 mm, and the seemingly different magnet thicknesses between the 10-pole and 14-pole machines is due to scaling effect. It can be seen that in the modular SPM machines, except the edges which have been

demagnetized due to adjacent magnets, the highest demagnetization within the chosen magnet due to armature field often occurs along the central line of the magnet. Therefore, the nodal analysis has been adopted for the demagnetization analysis, as shown in Fig. 6. Eleven nodes have been chosen and they divide the central line of the magnet by 10 equal segments.

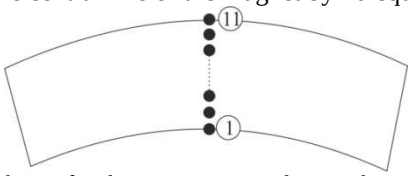

Fig. 6 Nodes chosen for demagnetization analysis within one magnet that experiences the highest demagnetization. Node 1 is the inner node adjacent to rotor core outer surface, node 11 is the outer node adjacent to the air-gap.

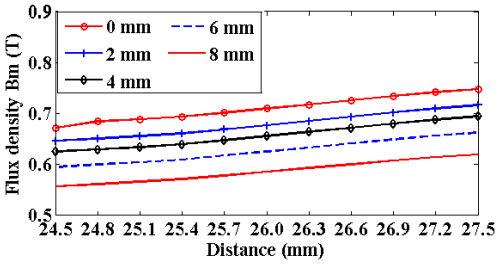

(a)

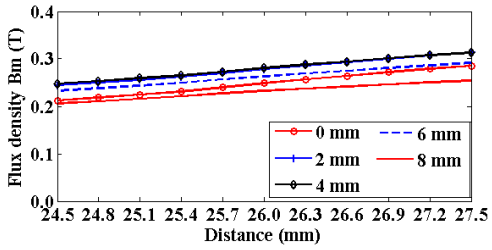

(b)

Fig. 7 B_m along the central line of one PM that experiences the highest demagnetization. The machine has 12-slot/10-pole. The distance of 24.5mm is corresponding to the node 1 while the distance of 27.5mm is corresponding to the node 11. (a) I_d = -4A, (b) I_d = -16A.

For different I_d and flux gap widths, the flux densities at different nodes have been calculated using 2D FEM, as shown in Fig. 7. Here, the 12-slot/10-pole modular machine has been chosen as an example. It is apparent that when I_d changes from -4A to -16A, flux densities at all nodes reduce accordingly. This can be explained by using (3) since the increase in flux density due to armature current (negative if the flux density due to PM is positive) will lead to an overall reduction in magnet flux density. It is also apparent that the node 1 has the highest demagnetization while the node 11 has the lowest demagnetization. When it comes to different flux gap widths, their influence on demagnetization is more complex. For lower I_d, e.g. -4A, the presence of flux gaps aggravates the demagnetization. However, at higher I_d, e.g. -16A, the smaller flux gaps can release the demagnetization while larger flux gaps will again aggravate the demagnetization at all nodes. This is mainly due to the influence of flux gaps on both the flux density due to magnets only and that due to armature field only, as detailed in APPENDIX (see Fig. 19).

B. Influence of Slot/Pole Number Combinations

For completeness, other modular machines with different slot/pole number combinations have also been investigated. By way of example, the flux densities at node 1 for the 12-slot/8-pole and 12-slot/16-pole modular machines are shown in Fig. 8. It is apparent that if the 2p is small, 2p smaller than N_s in particular, such as 12-slot/8-pole and 12-slot/10-pole, etc., the flux gaps tend to deteriorate the magnet demagnetization withstand capability. However, opposite trend has been observed for machines having higher 2p, 2p greater than N_s in particular, such as 12-slot/14-pole and 12-slot/16-pole, etc.

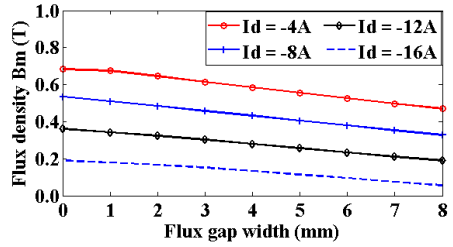

(a)

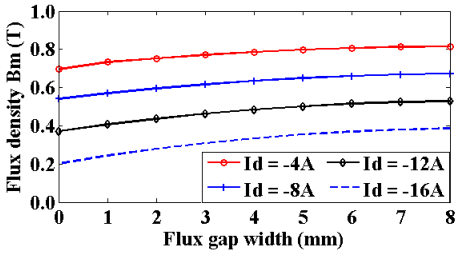

(b)

Fig. 8 B_m at node 1 vs FG and I_d. (a) 12-slot/8-pole, (b) 12-slot/16-pole.

C. Influence of PM Thickness

As described by (3), the thickness of magnet (l_m) is of significant importance for magnet demagnetization withstand capability. It is well established that the thicker the magnets, the higher the demagnetization withstand capability. This is also validated by the results shown in Fig. 9.

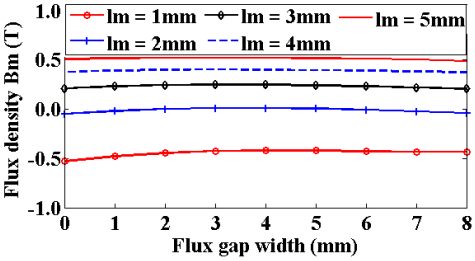

(a)

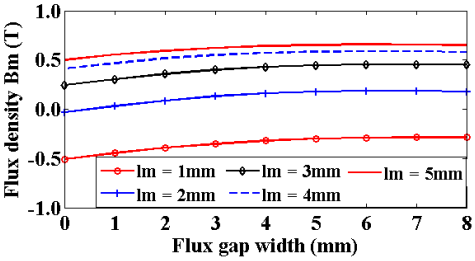

(b)

Fig. 9 B_m at the point 1 vs flux gap width and magnet thickness. I_d = -16A. (a) 12-slot/10-pole, (b) 12-slot/14-pole.

It is apparent that although the flux densities at node 1 increases with the increasing magnet thickness, the trends of flux density as a function of flux gap width do not change for both the 12-slot/10-pole and 12-slot/14-pole modular machines. Similar effect has been found for the air-gap length, and therefore, not shown here. For machines with thinner magnets, e.g. l_m = 1 mm or 2 mm, the irreversible demagnetization [min flux density < -0.08T (Knee point at 20°C)] could occur if the flux gap width is not carefully selected.

D. Influence of Machine Operating Temperature

The previous results are only for one temperature (20°C). However, machine operating temperature has a significant impact on the magnet remanence, knee point, etc. and hence on the magnet demagnetization withstand capability. Therefore, the following section is devoted to investigate this influence. Two typical operating temperatures have been chosen, i.e. 75°C and 150°C, which covers the operating temperatures for most applications. The corresponding magnet knee points and remanences are given in TABLE II. It is worth mentioning that for simplicity, the temperature distribution within one magnet is assumed to be uniform.

TABLE II NDFEB MAGNET CHARACTERISTICS AT DIFFERENT OPERATING TEMPERATURES

Temperature	Remanence (B_r)	Knee point
75 °C	1.127	0.2 (T)
150 °C	1.028	0.5 (T)

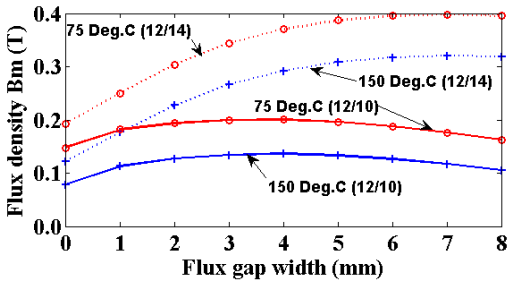

Fig. 10 B_m at node 1 vs flux gap width for different temperature and different slot/pole number combinations. I_d = -16A and l_m = 3mm.

To simplify the analysis, the demagnetization characteristics [2nd quadrant of magnet B(H) curve] of magnets are assumed to be linear at different temperatures. Under this assumption, the flux densities at node 1 of the magnet have been calculated again for the aforementioned temperatures, and compared in Fig. 10. It is apparent that the increasing temperature will inevitably aggravate the irreversible demagnetization of both modular machines, as expected. However, using flux gaps can always release the demagnetization of the 12-slot/14-pole machine while this effect is slight for the 12-slot/10-pole machine.

E. Modular SPM Machine with Defective Rotor

As established previously, different factors can lead to the demagnetization of PMs. However, in practice, it is difficult to assess the severity of demagnetization as well as its influence on the electromagnetic performance with the machines have the healthy rotors. In other words, the partial PM demagnetization phenomenon is uncontrollable and difficult to be simulated by the FE model. Therefore, in this paper, a 12-slot modular PM machine with a defective rotor, as shown in Fig. 13 (c), has been introduced as a controllable substitute in order to simulate the partial PM demagnetization. It is worth noting that the rotor shown in Fig. 13 (c) is a 10-pole surface mounted PM rotor with half of a N-pole magnet removed.

The 3D FE model of 12-slot modular PM machine with the aforementioned defective rotor has been built and simulated. The color maps of the open-circuit flux density of the modular PM machine with defective rotor are shown in Fig. 11. It is evident that the open-circuit air-gap flux density becomes asymmetric and a near zero flux density zone can be observed for the area with magnet removed, as shown in Fig. 11 (b). By employing such a 3D model of modular PM machine with defective rotor, the influence of PM partial demagnetization on the electromagnetic performance can be easily investigated. In Fig. 12, the output torques of modular PM machines having healthy and defective rotors are compared. It can be seen that when magnet is defective or partially demagnetized, the average torque will be significantly reduced while torque ripple increases.

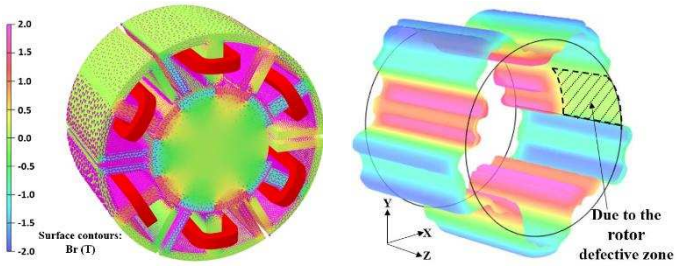

(a) (b)

Fig. 11 The color maps of open-circuit flux density. (a) Entire model. (b) Middle of the air-gap.

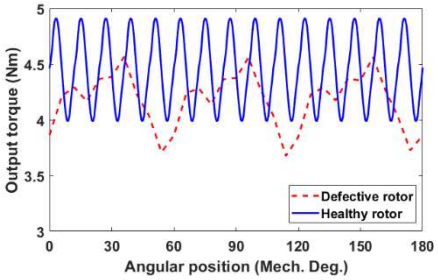

Fig. 12 The 3D FE results of the on-load torques of the modular PM machines with the healthy and defective rotors.

IV. Experimental Validation

In order to validate the previous FE predictions, the prototypes of modular PM machines having healthy and defective rotors have been built and tested, as shown in Fig. 13.

(a) (b) (c)

Fig. 13 The prototype 12-slot/10-pole modular PM machines. (a) The modular stator, (b) the healthy rotor, (c) the defective rotor.

A. Modular SPM Machines with Healthy Rotor

In this section, the main parameters to be measured are the d-axis inductance and the peak steady-state short-circuit current. The machine has healthy rotor, as shown in Fig. 13. To obtain the measured d-axis inductance, the self and mutual inductances can be obtained firstly by employing (4),

$$\begin{cases} L_{i(\theta)} = \dfrac{\sqrt{(V_i/I_i) - R^2}}{2\pi f} \\ M_{ij(\theta)} = \dfrac{V_j}{2\pi f} \end{cases} \quad (4)$$

where V_i, I_i and V_j are the amplitudes of the measured phase voltage and current in phase i and the amplitude of phase voltage in phase j respectively. R is the measured phase resistance which is 1.4 Ω for the prototype machine. The frequency f of the sinusoidal voltage of the phase A is set to be 100Hz during the experiment to achieve good signal to noise ratio and also to avoid high iron losses that would influence the measurement accuracy. The predicted and measured self- and mutual-inductances are compared in Fig. 14. The predictions are based on 3D FE model, similar to that shown in Fig. 11, and hence, the end-winding effect can be taken into account.

Then, (5) can be employed to derive the d-axis inductance [17]. To be consistent, this has been carried out for both the predicted and measured d-axis inductances.

$$L_d = L_0 - M_0 + \left(\frac{L_2}{2} + M_2\right) \quad (5)$$

where L_0 and M_0 are the dc components of the self- and mutual-inductances, respectively. L_2 and M_2 are the 2nd order harmonics in the self- and mutual-inductances, respectively.

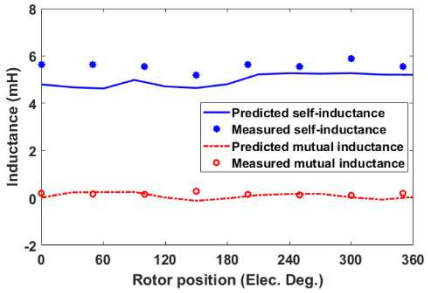

Fig. 14 Predicted and measured self- and mutual-inductances of the modular PM machine.

The predicted and measured d-axis inductances have been derived, and compared in Table III, in which the predicted and measured short-circuit currents at room temperature (~20°C) are also given.

Table III PREDICTED AND MEASURED L_D AND STEADY-STATE I_{SC} FOR 12-SLOT/10-POLE AND 12-SLOT/14-POLE MODULAR MACHINES

	12-slot/10-pole	12-slot/14-pole
L_d (mH)	5.81 (predicted)/5.78 (measured)	
I_{SC} (A)	10.18 (predicted) 10.5 (measured)	8.81 (predicted) 9 (measured)

B. Experimental Validation on the Modular PM Machine with Defective Rotor

a. Phase back-EMF

At the rated speed (400rpm), the back-EMF of phase A of the 12-slot modular PM machine with the healthy and defective rotors has been calculated by FE and validated by tests, as shown in Fig. 15.The defective rotor changes the periodicity of the phase back-EMF and introduce extra harmonic contents that do not exist in the machines with healthy rotor, such as, 1st, 2nd order harmonics, etc. Moreover, the beginning part of the EMF is lower due to the defective magnet.

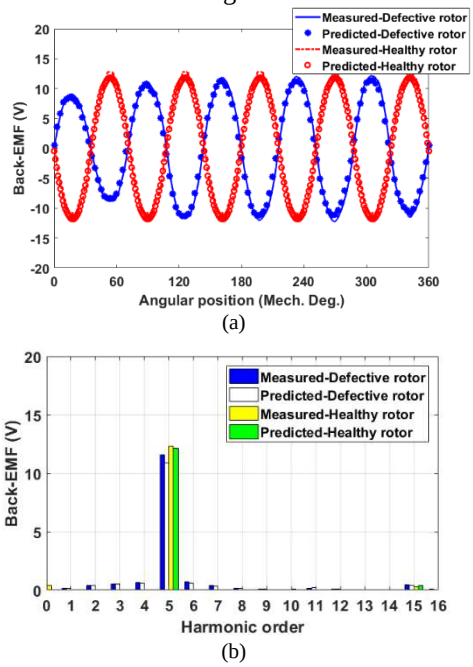

Fig. 15 Predicted and measured back-EMFs of the modular PM machine with the healthy and defective rotors. (a) Waveforms. (b) Spectra.

b. Cogging Torque and Static Torque

The method of measuring static torque and cogging torque is described in [18] and the test rig is illustrated in Fig. 16. The rotor shaft is connected to a balance beam which provides the possibility of using the digital scale to measure the force produced by the prototype. Hence, by doing so, the rotor needs to be stationary while the stator is rotated instead to vary the rotor position. As a result, both the cogging torque and the static torque can be measured for different rotor positions.

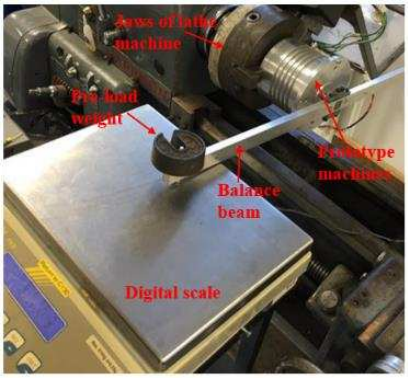

Fig. 16 Test rig for static torque and cogging torque measurements.

Fig. 17 shows the measured and predicted cogging torques of the modular PM machine with defective and healthy rotors. It has been established that the cogging torque of modular PM machine is mainly determined by the factor N_{cm}, which is the least common multiple of the rotor pole number $(2p)$ and the flux gap number (N_{FG}) [19]. For the healthy rotor case, N_{cm} equals to 30 if N_{FG} is 6 and $2p$ is 10, and hence, there are 5 cogging torque periods within 60 Mech. Deg., which is shown in Fig. 17 as the dash line. However, for the case of defective rotor, the value of N_{cm} becomes 6 since the rotor is asymmetric. Therefore, the periodicity of cogging torque is 60 Mech. Deg., as shown by the solid line in Fig. 17. Furthermore, the peak-to-peak cogging torque of modular PM machine with defective rotor is bigger than that of the modular PM machine with healthy rotor. This is mainly due to its asymmetric rotor and hence smaller N_{cm}.

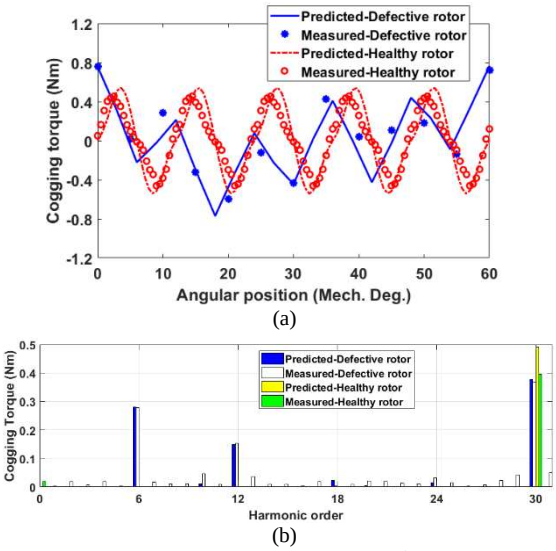

Fig. 17 Predicted and measured cogging torques of the modular PM machine with healthy and defective rotors. (a) Waveforms. (b) Spectra.

Similarly, the on-load static torque can be measured by supplying the prototype with DC currents ($I_A = I, I_B = I_C = -I/2$, with I = 3A). The predicted and measured static torques of modular PM machines with healthy and defective rotors are shown in Fig. 18. It can be seen that the static torque with defective rotor is smaller while has larger ripple mainly due to the reduction in phase back-EMF (see Fig. 15) while increase in cogging torque (see Fig. 17)

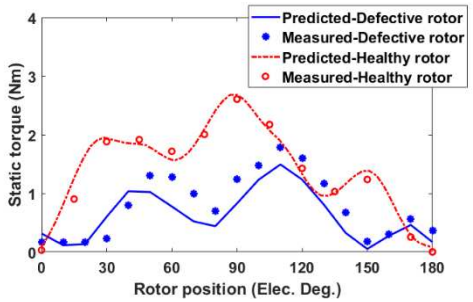

Fig. 18 Predicted and measured static torque of the modular PM machine ($I_A = 3A$). 3A DC current is chosen to avoid machine overheating.

V. Conclusions

This paper investigates the irreversible demagnetization withstand capabilities of modular surface mounted permanent magnet machines. The influence of armature field, flux gap width, slot/pole number combination, magnet thickness and operating temperature, etc. on magnet demagnetization has been investigated. It is found that the flux gaps have significant impact on magnet demagnetization, i.e. for small pole number, particularly the pole number smaller than slot number, the flux gaps tend to aggravate the magnet demagnetization. However, for large pole number, in particular the pole number greater than slot number, the flux gaps can significantly mitigate the magnet demagnetization. This is also true for different temperatures and magnet thicknesses.

The d-axis inductance and relevant short-circuit current have been predicted and also validated by measurements. Moreover, the modular PM machine with a defective rotor has been introduced to represent the partial demagnetization conditions in a controllable way. The experimental validations such as phase back-EMF, cogging torque, static torque have been carried out to investigate the influence of partial demagnetization on machine performances.

Appendix

Using the aforementioned FP method, the influence of flux gaps on flux density due to magnets only and that due to armature field only can be analyzed separately. Since the node 1 often experiences the highest demagnetization along the central line of the aforementioned magnet, it will be chosen for the following analysis. Similar to on-load flux linkages due to magnets only [see Fig. 3 (a)], the flux density due to magnets only at node 1 of the 12-slot/14-pole increases to its maximum then declines slightly thereafter, as shown in Fig. 19 (a). However, it decreases steadily for the 12-slot/10-pole machine. This is mainly due to the fact that the flux gaps act as a filter, which increases the on-load magnet flux density due to magnets only for the 12-slot/14-pole machine while reduces that for the 12-slot/10-pole machine.

The flux densities due to armature field only at node 1 are similar for both the 12-slot/10-pole and 12-slot/14-pole machines, as shown in Fig. 19 (b). It is apparent that when flux gap width increases, the absolute value of flux density due to armature field reduces for different I_d. This is mainly due to the fact that when flux gap width increases, the effective air-gap length increases, thus β in (3) reduces as well. As a result, the flux density term in (3) related to armature field (NI) will reduce accordingly.

The aforementioned influence of flux gaps on both the flux densities due to magnets only and due to armature field only leads to the resultant flux density variations shown in Fig. 19 (c) and (d), for the 12-slot/10-pole and 12-slot/14-pole machines, respectively. It is found that for the 12-slot/10-pole machine, only at high I_d (-16A), its demagnetization withstand capability can be slightly improved if the flux gap width is properly chosen. However, it is apparent that for the 12-slot/14-pole machine, the flux density at node 1 always increases with the increasing flux gap width, so its demagnetization withstand capability always improves.

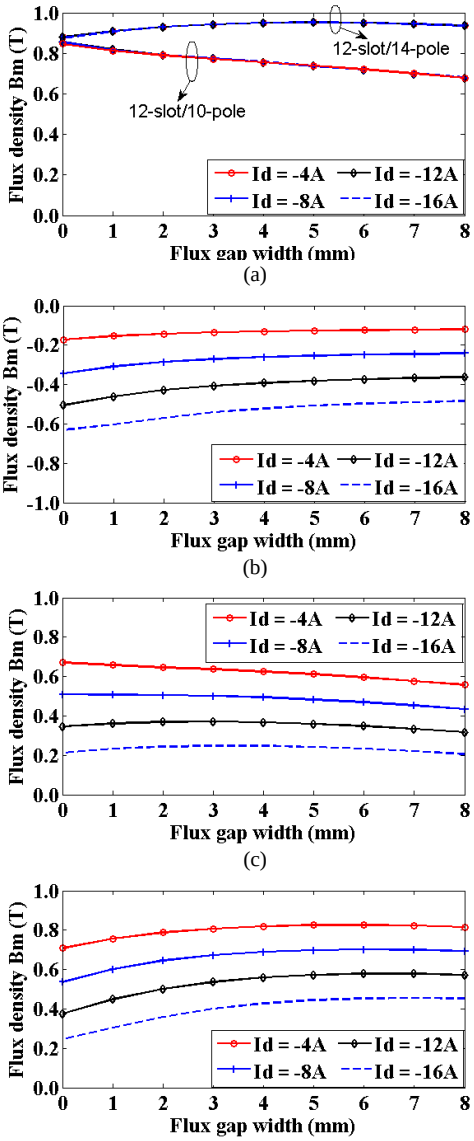

Fig. 19 B_m at the node 1 vs flux gap width and I_d. (a) PMs only, (b) armature field only (12/10 and 12/14), (c) total (12/10), (d) total (12/14).

REFERENCES

[1] E. Spooner, A. C. Williamson and G. Catto, "Modular design of permanent-magnet generators for wind turbines," IEE Proc. Elec. Power Appl., vol. 143, no. 5, pp. 388-395, Sep. 1996.

[2] M. J. Jin, C. F. Wang, J. X. Shen and B. Xia, "A modular permanent-magnet flux-switching linear machine with fault-tolerant capability," IEEE Trans. Magn., vol. 45, no. 8, pp. 3179-3186, Aug. 2009.

[3] G. Dajaku and D. Gerling, "Low costs and high-efficiency electric machines," in 2nd Int. Elec. Drives Production Conf. (EDPC), 15-18 Oct. 2012.

[4] G. J. Li, Z. Q. Zhu, M. P. Foster and D. A. Stone, "Comparative studies of modular and unequal tooth pm machines either with or without tooth tips," IEEE Trans. Mag., vol. 50, no. 7, pp. 1-10, Jul. 2014.

[5] H. Akita, Y. Nakahara, N. Miyake, and T. Oikawa, "New core structure and manufacturing method for high efficiency of permanent magnet motors," in Proc. 38th IAS Annu. Meet. Conf. Record Ind. Appl. Conf, Oct. 2003.

[6] Z. Q. Zhu, Z. Azar and G. Ombach, "Influence of additional air gaps between stator segments on cogging torque of permanent-magnet machines having modular stators," IEEE Trans. Magn., vol. 48, no. 6, pp. 2049-2055, Jun. 2012.

[7] H. Xiong, J. Zhang, M. W. Degner, C. Rong, F. Liang and W. Li, "Permanent-magnet demagnetization design and validation," IEEE Trans. Ind. Appl., vol. 52, no. 4, pp. 2961-2970, Jul/Aug. 2016.

[8] G. Choi and T. M. Jahns, "Interior permanent magnet synchronous machine rotor demagnetization characteristics under fault conditions," in 2013 IEEE Energy Conversion Congress and Exposition (ECCE), 15-19 Sept. 2013.

[9] J. D. McFarland and T. M. Jahns, "Investigation of the rotor demagnetization characteristics of interior pm synchronous machines during fault conditions," IEEE Trans. Ind. Appl., vol. 50, no. 4, pp. 2768-2775, Jul.-Aug. 2014.

[10] K. Lee, C. Jin and J. Lee, "Local demagnetisation analysis of a permanent magnet motor," IET Electr. Power. Appl., vol. 9, no. 3, pp. 280-286, Mar. 2015.

[11] J. Faiz and E. Mazaheri-Tehrani, "Demagnetization modeling and fault diagnosing techniques in permanent magnet mchines under stationay and nonstationary onditions: an oveview," IEEE Trans. Ind. Appl., vol. 53, no. 3, pp. 2772-2785, May/Jun. 2017.

[12] D. D. Reigosa, D. Fernandez, T. Tanimoto, T. Kato and F. Briz, "Permanent-magnet temperature distribution estimation in permanent-magnet synchronous machines using back electromotive force harmonics," IEEE Trans. Ind. Appl., vol. 52, no. 4, pp. 3093-3103, Jul./Aug. 2016.

[13] G. J. Li and Z. Q. Zhu, "Demagnetization of modular surface mounted permanent magnet machines," in 2016 XXII International Conference on Electrical Machines (ICEM), Lausanne, Switzerland, 4-7/Sept./2016.

[14] V. I. Patel, J. B. Wang and S. S. Nair, "Demagnetization assessment of fractional-slot and distributed wound 6-phase permanent magnet machines," IEEE Trans. Magn., vol. 51, no. 6, pp. 1-11, Jun. 2015.

[15] W. Q. Chu and Z. Q. Zhu, "Average torque separation in permanent magnet synchronous machines using frozen permeability," IEEE Trans. Magn., vol. 49, no. 3, pp. 1202-1210, Mar. 2013.

[16] James L. and Kirtley Jr., "6.685 Electric Machines," Massachusetts Institute of Technology, Cambridge, MA, 2005.

[17] A. E. Fitzgerald, C. Kingsley, and S. D. Umans, Electric Machinery, New York: McGraw-Hill, 1989.

[18] Z. Q. Zhu, "A simple method for measuring cogging torque in permanent magnet machines," in IEEE Power & Energy Society General Meeting, 26-30 Jul. 2009.

[19] G. J. Li, B. Ren, Z. Q. Zhu, Y. X. Li and J. Ma, "Cogging torque mitigation of modular permanent magnet machines," IEEE Trans. Magn., vol. 52, no. 1, pp. 1-10, Jan. 2016..